

Prescribed-Time Boresight Control of Spacecraft Under Pointing Constraints

Xiaodong Shao, *Member, IEEE*, Haoyang Yang, *Member, IEEE*, Haoran Li, Zongyu Zuo, *Senior Member, IEEE*, Jose Guadalupe Romero, *Member, IEEE*, and Qinglei Hu *Senior Member, IEEE*

Abstract—This article proposes an integrated boresight guidance and control (IBGC) scheme to address the boresight reorientation problem of spacecraft under temporal and pointing constraints. A C^1 continuous, saturated prescribed-time adjustment (PPTA) function is presented, along with the establishment of a practical prescribed-time stability criterion. Utilizing the time scale transformation technique and the PPTA function, we propose a prescribed-time guidance law that guides the boresight vector from almost any initial orientation in free space to a small neighborhood of the goal orientation within a preassigned time, while avoiding all forbidden zones augmented with safety margins. Subsequently, a prescribed-time disturbance observer (PTDO) is derived to reconstruct the external disturbances. By leveraging barrier and PPTA functions, a PTDO-based reduced-attitude tracking controller is developed, which ensures prescribed-time boresight tracking within a “safe tube”. By judiciously setting the safety margins, settling times, and safe tube for the guidance and control laws, the proposed IBGC scheme achieves pointing-constrained boresight reorientation within a required task completion time. Simulation and experimental results demonstrate the efficacy of the proposed IBGC scheme.

Index Terms—Reduced attitude, prescribed-time control, disturbance observer, pointing constraints.

I. INTRODUCTION

REORIENTING the boresight axis of light-sensitive payloads (e.g., telescopes, cameras, and star trackers) toward a specified direction is an essential function of many spacecraft. Extensive research has explored three-axis attitude control techniques applicable to spacecraft boresight reorientation [1]–[5] (just to name a few). Most existing studies formulate the attitude control problem within the framework of Special Orthogonal Group $SO(3)$, or utilizing various attitude parameterizations that can be Euclidean, such as Euler angles and Rodrigues parameters defined in \mathbb{R}^3 , or non-Euclidean, such as unit quaternions defined on the three-sphere \mathbb{S}^3 . These attitude representations necessitate knowledge of the spacecraft’s full attitude. However, in pointing applications, rotations about the body-fixed boresight axis are usually irrelevant, rendering full attitude information unnecessary. Motivated by this fact, Bullo

et al. [6] introduced the reduced-attitude representation on the unit 2-sphere \mathbb{S}^2 to address the boresight reorientation problem. This solution requires only a single boresight vector and three-axis angular velocity measurements. Chaturvedi et al. [7] proposed a simple proportional-derivative (PD) controller for reduced-attitude stabilization of rigid bodies. Pong and Miller [8] presented reduced-attitude guidance and control laws to achieve pointing, tracking, and searching tasks.

In pointing applications – whether for target pointing, inertial stabilization, or interplanetary missions – spacecraft are typically required to protect onboard light-sensitive payloads from direct exposure to bright objects (e.g., the Sun or the illuminated sides of the Earth) to avoid functional damage [9]. For example, the James Webb Space Telescope (JWST) must ensure that its infrared instruments avoid direct exposure to the Sun, a critical requirement for maintaining a low-temperature condition necessary for high-precision spectral observations. This requirement imposes pointing constraints on the boresight control, which can be mathematically described as a keep-out cone centered on the direction of the forbidden zone. Existing solutions to the pointing-constrained boresight control problem can generally be classified into two categories: artificial potential function (APF)-based methods [10]–[12] and path planning methods [13]–[15]. The APF-based methods, comprising an attractive potential for motion-to-go and a repulsive potential for pointing avoidance, can generate analytical control laws that are both computationally efficient and easy to implement. Hu et al. [16] and Shao et al. [17] designed two APF-based reduced-attitude control approaches for spacecraft boresight tracking and reorientation, explicitly accounting for pointing and angular velocity constraints. Recently, Liu et al. [18] addressed the reduced-attitude boresight control problem under elliptical pointing constraints, employing the navigation function – a specialized form of APFs. As is well known, the APF-based methods are prone to the local minima problem, which may cause the boresight vector to get trapped in a local minimum, thereby hindering global convergence to the desired orientation. Although the planning methods are free from local minima, they tend to be computationally intensive and demand substantial computing and storage resources.

Nearly all of the aforementioned attitude control approaches achieve only asymptotic convergence of the boresight vector to the desired orientation as time approaches infinity. This is inadequate for time-critical spacecraft reorientation missions, which must be completed within a specified finite time window. Finite/fixed-time control techniques can enable system states to converge to zero within a finite time upper bounded by

Corresponding author: Qinglei Hu

X. Shao, Z. Zuo, and Q. Hu are with the School of Automation Science and Electrical Engineering, Beihang University, Beijing 100191, China (E-mail: xdshao_sasee@buaa.edu.cn; zzybobby@buaa.edu.cn; huql_buaa@buaa.edu.cn).

H. Yang is with the School of Engineering, University of Warwick, Coventry CV4 7AL, UK (E-mail: haoyang.yang@warwick.ac.uk).

H. Li is with the International Innovation Institute, Beihang University, Hangzhou 311115, China (E-mail: haoranli@buaa.edu.cn).

J. G. Romero is with the Departamento Académico de Ingeniería Eléctrica y Electrónica, Instituto Tecnológico Autónomo de México (ITAM), Mexico City, Mexico (E-mail: jose.romerovelazquez@itam.mx).

a computable value [19], offering effective solutions for time-critical boresight control problems. Various finite/fixed-time control approaches have been reported for spacecraft attitude stabilization or tracking, incorporating techniques such as sliding mode control and backstepping control (see, indicatively, [20]–[22]). In particular, Li et al. [22] designed a fixed-time attitude controller to achieve pointing-constrained spacecraft reorientation, by constructing a novel APF-based sliding mode variable. A significant drawback of finite/fixed-time control is that the upper bound on settling time is often overestimated, resulting in unnecessarily large control efforts. Recently, a new finite-time control paradigm, known as prescribed-time control, has been proposed, which allows designers to arbitrarily specify the convergence time in advance. In [23], a continuous sliding mode controller was developed to achieve predefined-time stabilization of robotic manipulators. Yucelen et al. [24] provided an alternative approach for the design of prescribed-time control by introducing a time scale transformation (TST) function. It is noteworthy that TST functions introduce a time-varying gain into the prescribed-time control law, referred to as prescribed-time adjustment (PTA) function [25]. The PTA function tends to infinity as time approaches the prescribed settling time, which inevitably causes a singularity problem. The lead switching strategy has been widely used to avoid the potential singularity (e.g., see [26]–[28]). However, this results in a PTA function that is either discontinuous or continuous but not differentiable, limiting its application to the prescribed-time control for high-order systems. These existing prescribed-time control methods, on the other hand, lack the capability to handle pointing constraints.

To the best of the authors’ knowledge, no existing results achieve boresight reorientation of spacecraft under temporal and pointing constraints. To bridge this gap, we propose an integrated boresight guidance and control (IBGC) scheme, using a newly-constructed PTA function. By judiciously setting the safety margins, settling times, and “safe tube” for the guidance and control laws, the proposed IBGC scheme ensures that the boresight vector converges to a small neighborhood of the desired orientation within a required task completion time, while avoiding all forbidden pointing zones. The proposed method is validated through simulation and experimental results. The main contributions of this article are three-fold:

- 1) A C^1 continuous, saturated PTA (termed PPTA) function is designed and incorporated into the IBGC framework to achieve prescribed-time boresight control, while a sufficient condition (i.e., Lemma 1) for practical prescribed-time stability is established in the Lyapunov sense. This function, along with Lemma 1, can be readily applied to the design of observers, estimators, and controllers with practical prescribed-time convergence.
- 2) An APF-based boresight guidance law is proposed, utilizing the TST technique recently introduced in [24] and the newly-constructed PPTA function. This guidance law generates a smooth reference trajectory that, starting from almost any initial orientation in free space, converges to a small neighborhood of the desired orientation within a prescribed time, while avoiding all forbidden

pointing zones augmented by safety margins.

- 3) A PPTA function-based prescribed-time disturbance observer (PTDO) is developed to reconstruct external disturbances. Then, by leveraging barrier and PPTA functions, a PTDO-based reduced-attitude controller is proposed for boresight tracking. The resulting controller ensures practical prescribed-time convergence of attitude and angular velocity tracking errors, while maintaining the attitude error within a predefined “safe tube”, even in the presence of external disturbances.

The remainder of this article is organized as follows. Section II presents a novel PPTA function, outlines the mathematical preliminaries, and formulates the boresight reorientation problem. In Section III, an IBGC scheme is proposed, accompanied by detailed designs and analyses of prescribed-time boresight guidance and control laws. Sections IV and V provide simulation and experimental results, respectively, to demonstrate the efficacy of the proposed method. Finally, Section VI concludes the article and outlines directions for future work.

II. PRELIMINARIES AND PROBLEM FORMULATION

A. Notations

Throughout the paper, \mathbf{I}_n is the $n \times n$ identity matrix, and $\|\cdot\|$ denotes the 2-norm of a vector or the induced matrix norm. The special orthogonal group is denoted by $SO(3) := \{\mathbf{R} \in \mathbb{R}^{3 \times 3} \mid \mathbf{R}^\top \mathbf{R} = \mathbf{I}_3, \det(\mathbf{R}) = 1\}$. The unit 2-sphere, defined as $\mathbb{S}^2 := \{\mathbf{x} \in \mathbb{R}^3 \mid \|\mathbf{x}\| = 1\}$, is a 2-dimensional manifold embedded in \mathbb{R}^3 . We denote by $d_{\mathbb{S}^2}(\mathbf{x}, \mathbf{y}) := \arccos(\mathbf{x}^\top \mathbf{y})$ the geodesic distance between any two points $\mathbf{x}, \mathbf{y} \in \mathbb{S}^2$. Given a non-empty subset $\mathcal{A} \subset \mathbb{R}^n$, the topological interior of \mathcal{A} is denoted by $\text{int}(\mathcal{A})$. The geodesic distance from a vector $\mathbf{x} \in \mathbb{S}^2$ to the set \mathcal{A} is defined as $d_{\mathcal{A}}(\mathbf{x}) := \inf\{d_{\mathbb{S}^2}(\mathbf{x}, \mathbf{y}) \mid \mathbf{y} \in \mathcal{A}\}$. The cross product operator $[\cdot]_{\times} : \mathbb{R}^3 \rightarrow \mathbb{R}^{3 \times 3}$ is defined such that $[\mathbf{x}]_{\times} \mathbf{y} = \mathbf{x} \times \mathbf{y}$ for any $\mathbf{x}, \mathbf{y} \in \mathbb{R}^3$, which complies with the following properties:

$$\begin{aligned} \mathbf{y}^\top [\mathbf{y}]_{\times} &= \mathbf{0}, [\mathbf{y}]_{\times} \mathbf{y} = \mathbf{0} \\ [\mathbf{y}]_{\times}^\top &= -[\mathbf{y}]_{\times}, [\mathbf{y}]_{\times} \mathbf{z} = -[\mathbf{z}]_{\times} \mathbf{y} \\ [\mathbf{y}]_{\times}^2 &= \mathbf{y} \mathbf{y}^\top - \|\mathbf{y}\|^2 \mathbf{I}_3, [\mathbf{R} \mathbf{y}]_{\times} = \mathbf{R} [\mathbf{y}]_{\times} \mathbf{R}^\top \end{aligned}$$

for any $\mathbf{y}, \mathbf{z} \in \mathbb{R}^3$ and any $\mathbf{R} \in SO(3)$. In particular, when $\mathbf{y} \in \mathbb{S}^2$, it follows that

$$[\mathbf{y}]_{\times}^2 = \mathbf{y} \mathbf{y}^\top - \mathbf{I}_3, [\mathbf{y}]_{\times}^3 = -[\mathbf{y}]_{\times}.$$

B. A New PTA Function

Definition 1: [29] Consider the following system:

$$\dot{\mathbf{y}}(t) = \mathbf{f}(t, \mathbf{y}(t)), \mathbf{f}(t, \mathbf{0}) = \mathbf{0} \quad (1)$$

where $\mathbf{f} : \mathbb{R}^+ \times \mathbb{R}^n \rightarrow \mathbb{R}^n$ is a piecewise continuous in t and locally Lipschitz in \mathbf{y} . Let the solution of (1) be $\mathbf{y}(t; \mathbf{y}_0)$ with $\mathbf{y}_0 := \mathbf{y}(0)$. If the origin $\mathbf{y} = \mathbf{0}$ of (1) is Lyapunov stable, and there exists a constant $T > 0$ such that

$$\mathbf{y}(t; \mathbf{y}_0) = \mathbf{0}, \forall t \in [T, \infty)$$

then the origin of (1) is prescribed-time stable (PTS). Furthermore, if there exist $\varepsilon > 0$ and $T > 0$ such that

$$\|\mathbf{y}(t; \mathbf{y}_0)\| \leq \varepsilon, \forall t \in [T, \infty)$$

then the origin of (1) is termed practical PTS (PPTS).

Definition 2: A smooth function $\eta : [0, \infty) \rightarrow [0, T)$ is called a time scale transformation (TST) function if:

- 1) it is strictly increasing;
- 2) it is s.t. $\eta(0) = 0$ and $\eta'(0) = 1$;
- 3) it is s.t. $\lim_{s \rightarrow \infty} \eta(s) = T$ and $\lim_{s \rightarrow \infty} \eta'(s) = 0$.

In fact, a TST function $\eta(s)$ can transform the infinite-time interval $s \in [0, \infty)$ into a finite time interval $t \in [0, T)$. A typical choice of $\eta(s)$ is as follows:

$$\eta(s) = T(1 - e^{-\frac{s}{T}}). \quad (2)$$

Let $\eta'(s) := d\eta(s)/ds$ and define a prescribed-time adjustment (PTA) function $\mu_p : \mathbb{R}_{\geq 0} \rightarrow \mathbb{R}_{> 0}$ as

$$\mu_p(t) = \mu_p(\eta(s)) := \frac{1}{\eta'(s)} = \frac{T}{T-t}, \quad t \in [0, T) \quad (3)$$

which satisfies that $\mu_p(0) = 1$ and $\lim_{t \rightarrow T} \mu_p(t) = \infty$.

It is noteworthy that the prescribed-time controllers utilizing the PTA gain $\mu_p(t)$ cannot be practically implemented due to the unbounded nature of $\mu_p(t)$ as $t \rightarrow T$. The commonly-used lead switching approach (e.g., see [26]–[28]) ensures that the PTA function is well-defined for all $t \geq 0$, as described by

$$\mu_s(t) = \begin{cases} \mu_p(t), & \text{if } t \in [0, T^*] \\ 1 \text{ or } \mu_p(T^*), & \text{if } t \in [T^*, \infty) \end{cases}$$

where $T^* \in (0, T]$ is a switching time. However, this leads to a discontinuous PTA function, limiting its application in the design of prescribed-time controllers for second- or higher-order systems, since these typically require the PTA function to be at least C^1 continuous. To address these issues, we propose a C^1 continuous, saturated PTA function, referred to as PPTA function, defined as follows:

$$\mu(t) = \begin{cases} \mu_p(t), & \text{if } t \in [0, T^*] \\ \mu_p(T^*)\psi(t), & \text{if } t \in [T^*, T] \\ \frac{\pi+2}{\pi}\mu_p(T^*), & \text{if } t \in [T, \infty) \end{cases} \quad (4)$$

with

$$\psi(t) := \left[1 + \frac{2}{\pi} \sin\left(\frac{\pi}{2} \frac{t - T^*}{T - T^*}\right) \right].$$

Property 1: The newly-constructed PPTA function $\mu(t)$ satisfies the following properties:

- 1) it is C^1 continuous and bounded on $t \in [0, \infty)$;
- 2) it is monotonically increasing on $t \in [0, T]$;
- 3) its initial value satisfies $\mu(0) = 1$;
- 4) for all $t \geq T$, $\mu(t) = \left(1 + \frac{2}{\pi}\right) \frac{T}{T-T^*}$.

The properties of $\mu(t)$ described above are straightforward and can be clearly seen in Fig. 1. In the following, we establish a sufficient condition for PPTS of the system's origin.

Lemma 1: Consider the nonlinear system described by (1). Let $V : \mathbb{R}^n \rightarrow \mathbb{R}^+$ be a continuously differentiable, positive definite function, satisfying

$$\dot{V}(\mathbf{y}) \leq -\alpha\mu(t)V(\mathbf{y}) + \beta, \quad V(\mathbf{y}(0)) = V_0 \quad (5)$$

where both $\alpha > 1/T$ and $\beta \geq 0$ are constants, and $\mu(t)$ is a PPTA function defined in (4). Then, the origin of (1) is PPTS;

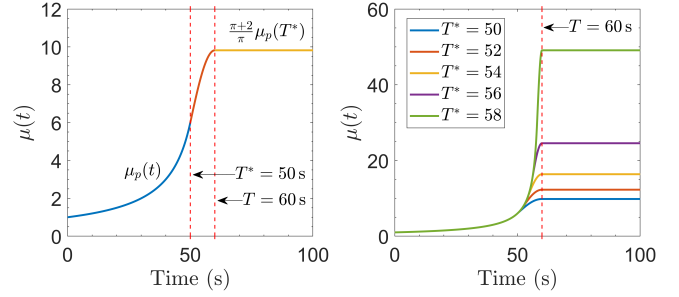


Fig. 1. Time history of $\mu(t)$: (a) the left subfigure illustrates a special case of $\mu(t)$ with $T^* = 50$ and $T = 60$; (b) the right subfigure depicts the time histories of $\mu(t)$ for different values of T^* .

specifically, the solution of (1) converges to the following set within the prescribed time T^* :

$$\Omega := \{\mathbf{y} \in \mathbb{R}^n \mid V(\mathbf{y}) \leq \max\{v_1, v_2\}\} \quad (6)$$

where v_1 and v_2 are given by

$$v_1 := \left(\frac{T - T^*}{T}\right)^{\alpha T} V_0 + \bar{v}_1, \quad v_2 := \frac{\beta(T - T^*)}{\alpha T} \quad (7)$$

with

$$\bar{v}_1 := \frac{\beta T}{\alpha T - 1} \left[\frac{T - T^*}{T} - \left(\frac{T - T^*}{T}\right)^{\alpha T} \right] > 0.$$

By choosing α and T^* such that $T - T^* \ll \alpha T - 1$, the set Ω can be arbitrarily reduced by increasing T^* closer to T .

Proof. The proof is relegated to Appendix A. \blacksquare

Remark 1: The PPTA function $\mu(t)$, along with Lemma 1, can be used to design prescribed-time state/disturbance observers, parameter estimators, and tracking controllers. Note that designing prescribed-time controllers for n -order systems typically requires the PPTA function to be C^{n-1} continuous. This limits the direct application of $\mu(t)$ to high-order systems, as it is only C^1 continuous. In such cases, the dynamic surface control approach presented in [30] can be used in conjunction with backstepping control. Additionally, while a higher value of $\mu(t)$ on $t \in [T^*, \infty)$ is instrumental for reducing the steady-state error bound, this may excite unmodeled high-frequency dynamics in practice, potentially leading to instability of the closed system. Therefore, for a prescribed time T , one should select an appropriate T^* to strike a balance between control accuracy and system stability.

C. Problem Formulation

Denote by $\mathbf{R} \in SO(3)$ and $\boldsymbol{\omega} \in \mathbb{R}^3$ the attitude and angular velocity of the body-fixed frame \mathcal{B} of a spacecraft with respect to (w.r.t.) an inertial frame \mathcal{N} , expressed in \mathcal{B} . The spacecraft attitude dynamics are described by

$$\dot{\mathbf{R}} = \mathbf{R}[\boldsymbol{\omega}]_{\times} \quad (8)$$

$$\mathbf{J}\dot{\boldsymbol{\omega}} = [\mathbf{J}\boldsymbol{\omega}]_{\times}\boldsymbol{\omega} + \mathbf{u} + \mathbf{d} \quad (9)$$

where $\mathbf{J} = \mathbf{J}^T \in \mathbb{R}^{3 \times 3}$ is the positive-definite inertia matrix of spacecraft, while $\mathbf{u} \in \mathbb{R}^3$ and $\mathbf{d} \in \mathbb{R}^3$ denote the control and disturbance torques, respectively. Let $\mathbf{b} \in \mathbb{S}^2$ be the boresight

vector of an onboard sensitive payload (e.g., telescope, camera or other instruments) resolved in the frame \mathcal{B} . We disregard the rotation about this axis and express it in the frame \mathcal{N} as $\mathbf{x} := \mathbf{R}\mathbf{b} \in \mathbb{S}^2$. The kinematics of \mathbf{x} is expressed as

$$\dot{\mathbf{x}} = [\boldsymbol{\Omega}]_{\times} \mathbf{x} \quad (10)$$

where $\boldsymbol{\Omega} := \mathbf{R}\boldsymbol{\omega}$ is the angular velocity expressed in \mathcal{N} . For any $(\mathbf{x}, \boldsymbol{\Omega}) \in \mathbb{S}^2 \times \mathbb{R}^3$, $[\boldsymbol{\Omega}]_{\times} \mathbf{x} \in \mathbf{T}_{\mathbf{x}}\mathbb{S}^2$, indicating that $\mathbf{x} \in \mathbb{S}^2$ always holds under the driftless kinematics (10).

Assumption 1: The disturbance torque \mathbf{d} is differentiable and bounded, and there exists an unknown constant $d_m > 0$ such that $\|\dot{\mathbf{d}}\| \leq d_m$.

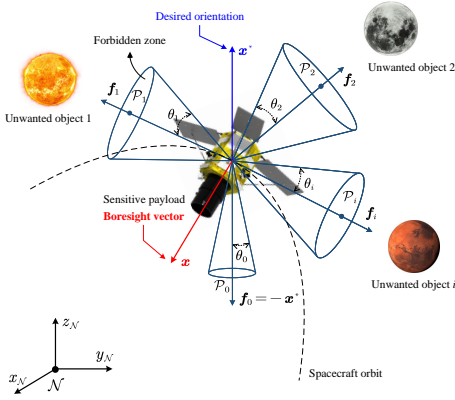


Fig. 2. Illustration of boresight pointing constraints.

During the boresight reorientation, it is necessary to ensure that the boresight axis of the on-board sensitive payload avoids bright objects, such as the Sun or the illuminated sides of the Earth and Moon. Suppose that there are $m \geq 1$ bright objects that the sensitive payload should avoid, resulting in m cone-shaped forbidden pointing zones, as illustrated in Fig. 2. The forbidden pointing constraints can be described in the inertial frame \mathcal{N} as follows:

$$\mathcal{P}_i := \{\mathbf{x} \in \mathbb{S}^2 \mid d_{\mathbb{S}^2}(\mathbf{x}, \mathbf{f}_i) \leq \theta_i\}, \quad i \in \mathbb{I} = \{0, 1, \dots, m\}$$

where $\mathbf{f}_i \in \mathbb{S}^2$ and $\theta_i \in (0, \pi/2)$ denote the center axis and half-angle of the i -th forbidden pointing cone, respectively. Note that \mathcal{P}_0 is a virtual forbidden zone around the antipodal point of the desired orientation \mathbf{x}^* (i.e., $\mathbf{f}_0 = -\mathbf{x}^*$). This zone is introduced to prevent \mathbf{x} from converging to the undesired equilibrium $-\mathbf{x}^*$ under a continuous controller. Then, the free space of the boresight vector \mathbf{x} is

$$\mathcal{F} := \mathbb{S}^2 \setminus \bigcup_{i=0}^m \mathcal{P}_i = \{\mathbf{x} \in \mathbb{S}^2 \mid d_{\mathbb{S}^2}(\mathbf{x}, \mathbf{f}_i) > \theta_i, \forall i \in \mathbb{I}\}.$$

To ensure that the boresight vector \mathbf{x} can fit freely between any of the forbidden zones, we make the following ‘‘isolated’’ constraint assumption:

Assumption 2: The forbidden pointing zones are separated from each other by a clearance of at least

$$d_{\mathbb{S}^2}(\mathbf{f}_i, \mathbf{f}_j) > \theta_i + \theta_j + 2\iota, \quad \forall i, j \in \mathbb{I}, \quad i \neq j$$

where $\iota \in (0, \pi/2)$ is a constant.

The problem to be addressed is summarized below:

Problem 1: Consider the spacecraft attitude dynamics given by (8) and (9) under Assumption 1, and suppose that the forbidden zones \mathcal{P}_i , $i \in \mathbb{I}$ satisfy Assumption 2. The control objective is to develop a controller \mathbf{u} that guides the boresight vector \mathbf{x} from an initial pointing $\mathbf{x}(0) \in \mathcal{F}$ to the goal pointing $\mathbf{x}^* \in \text{int}(\mathcal{F})$ (motion to goal) within a designer-specified time T , while ensuring that \mathbf{x} remains within the free space \mathcal{F} at all times (forbidden pointing avoidance), despite the presence of inertia uncertainties.

III. MAIN RESULTS

In this section, an IBGC scheme that incorporates the PPTA function, defined in (4), is proposed to address Problem 1. The block diagram of this scheme is shown in Fig.3, where the guidance module accounts for generating a smooth reference trajectory \mathbf{x}_r with pointing avoidance and practical prescribed-time convergence. While in the control module, a PTDO-based reduced-attitude controller is developed to achieve prescribed-time boresight tracking within a predefined ‘‘safe tube’’, with a radius no larger than the safety margin, even in the presence of external disturbances. In this context, the boresight vector \mathbf{x} will converge to \mathbf{x}^* within a required task completion time, while avoiding all forbidden zones.

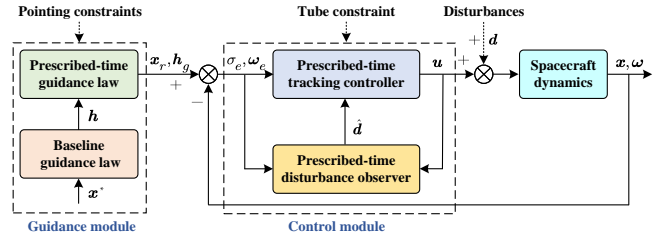


Fig. 3. Block diagram of the proposed IBGC scheme.

A. Prescribed-Time Boresight Guidance

Before proceeding, let $\mathbf{x}_r \in \mathbb{S}^2$ and $\boldsymbol{\Omega}_r \in \mathbb{R}^3$ denote, respectively, the reference boresight vector and angular velocity resolved in the inertial frame. As per (10), the kinematics of \mathbf{x}_r is expressed as

$$\dot{\mathbf{x}}_r = [\boldsymbol{\Omega}_r]_{\times} \mathbf{x}_r \quad (11)$$

with $\mathbf{x}_r(0) = \mathbf{x}(0)$ and $\boldsymbol{\Omega}_r(0) = \boldsymbol{\Omega}(0)$.

To enhance safety, a safety margin of size $\epsilon < \iota$ is defined around each forbidden zone \mathcal{P}_i , leading to $m + 1$ augmented forbidden zones

$$\mathcal{P}_i^\epsilon = \{\mathbf{x} \in \mathbb{S}^2 \mid d_{\mathbb{S}^2}(\mathbf{x}, \mathbf{f}_i) \leq \theta_i + \epsilon\}, \quad i \in \mathbb{I}$$

and an eroded free space $\mathcal{F}_\epsilon := \mathbb{S}^2 \setminus \bigcup_{i=0}^m \mathcal{P}_i^\epsilon$. Furthermore, an influence area is introduced for \mathcal{P}_i , defined as $\mathcal{I}_i := \{\mathbf{x} \in \mathbb{S}^2 \mid d_{\mathcal{P}_i}(\mathbf{x}) \leq \epsilon^*\}$ with

$$0 < \epsilon < \epsilon^* \leq \iota. \quad (12)$$

Bearing Assumption 2 and (12) in mind, the influence regions of different pointing constraints do not overlap. Thus, there is at most one forbidden pointing zone that can activate pointing avoidance at any given time. Note that ϵ^* should be chosen

such that \mathbf{x}^* lies outside the influence regions of all forbidden pointing constraints \mathcal{P}_i , $i \in \mathbb{I}$. As a stepping stone, we propose a baseline boresight guidance law that asymptotically guides \mathbf{x}_r toward the goal \mathbf{x}^* (motion to goal) from almost all initial orientations $\mathbf{x}_r(0) \in \mathcal{F}_\epsilon$, while ensuring forward invariance of the free space \mathcal{F}_ϵ (forbidden pointing avoidance).

Consider the following APF $U : \mathcal{F}_\epsilon \rightarrow \mathbb{R}^+$

$$U(\mathbf{x}_r) = \underbrace{k_a(1 - \mathbf{x}_r^\top \mathbf{x}^*)}_{\text{attractive potential}} + k_r \underbrace{\sum_{i=0}^m \phi_i(\mathbf{x}_r^\top \mathbf{f}_i)}_{\text{repulsive potential}} \quad (13)$$

where $k_a, k_r > 0$ are constants, and ϕ_i is a smooth repulsive function given by

$$\phi_i(z) = \begin{cases} (z - \varepsilon_i^*)^2 \ln \frac{\varepsilon_i - \varepsilon_i^*}{\varepsilon_i - z}, & \text{if } z \in [\varepsilon_i^*, \varepsilon_i) \\ 0, & \text{if } z \leq \varepsilon_i^* \end{cases}$$

with its gradient given by

$$\nabla \phi_i(z) = \begin{cases} 2(z - \varepsilon_i^*) \ln \frac{\varepsilon_i - \varepsilon_i^*}{\varepsilon_i - z} + \frac{(z - \varepsilon_i^*)^2}{\varepsilon_i - z}, & \text{if } z \in [\varepsilon_i^*, \varepsilon_i) \\ 0, & \text{if } z \leq \varepsilon_i^* \end{cases}$$

where $\varepsilon_i := \cos(\theta_i + \epsilon)$ and $\varepsilon_i^* := \cos(\theta_i + \epsilon^*)$. It is easy to verify that: 1) $\phi_i(z)$ is continuously differentiable; 2) $\phi_i(z)$ is strictly increasing on $z \in [\varepsilon_i^*, \varepsilon_i)$, with $\lim_{z \rightarrow \varepsilon_i} \phi_i(z) = +\infty$ and $\phi_i(z) = 0$ for all $z \leq \varepsilon_i^*$; 3) $\nabla \phi_i(z)$ is continuously differentiable and $\nabla \phi_i(z) \geq 0$ for all $z < \varepsilon_i$. As $\phi_i(\mathbf{x}_r^\top \mathbf{f}_i) \geq 0$ for all $\mathbf{x}_r^\top \mathbf{f}_i < \varepsilon_i$, the APF $U(\mathbf{x}_r)$ is positive definite on the practical free space \mathcal{F}_ϵ , and the equilibrium $\mathbf{x}_r = \mathbf{x}^*$ is the unique global minimum of $U(\mathbf{x}_r)$. The gradient of $U(\mathbf{x}_r)$ is derived as

$$\nabla U(\mathbf{x}_r) = -k_a \mathbf{x}^* + k_r \sum_{i=0}^m (\nabla \phi_i(\mathbf{x}_r^\top \mathbf{f}_i) \cdot \mathbf{f}_i). \quad (14)$$

Design the baseline guidance law as

$$\boldsymbol{\Omega}_r = \mathbf{h}(\mathbf{x}_r) := [\mathbf{x}_r]_\times^\top \nabla U(\mathbf{x}_r). \quad (15)$$

Substituting (15) into (10) yields

$$\dot{\mathbf{x}}_r = -[\mathbf{x}_r]_\times \mathbf{h}(\mathbf{x}_r) = -[\mathbf{x}_r]_\times [\mathbf{x}_r]_\times^\top \nabla U(\mathbf{x}_r). \quad (16)$$

Theorem 1: Consider the boresight kinematics described by (10). Suppose that the forbidden constraints \mathcal{P}_i , $i \in \mathbb{I}$ satisfy Assumption 2 and that their corresponding safety margin and influence region comply with (12). Then, the baseline guidance law $\boldsymbol{\Omega}_r = \mathbf{h}(\mathbf{x}_r)$ given by (15) guarantees that:

- 1) The practical free space \mathcal{F}_ϵ is forward invariant.
- 2) The boresight vector \mathbf{x}_r asymptotically converges to the desired equilibrium \mathbf{x}^* or reaches a set of m undesired critical points $\bigcup_{i=1}^m \{\mathbf{c}_i\}$ with \mathbf{c}_i satisfying

$$k_a [\mathbf{c}_i]_\times \mathbf{x}^* = k_r \nabla \phi_i(\mathbf{c}_i^\top \mathbf{f}_i) [\mathbf{c}_i]_\times \mathbf{f}_i. \quad (17)$$

Proof. The proof is relegated to Appendix B. ■

To achieve prescribed-time boresight guidance, inspired by [31], we propose a prescribed-time guidance law by incorporating a PPTA function $\mu_g(t)$ with design parameters T_g and T_g^* into the baseline law (15)

$$\boldsymbol{\Omega}_r = \mathbf{h}_g(\mathbf{x}_r, t) := \mu_g(t) \mathbf{h}(\mathbf{x}_r). \quad (18)$$

As $\mathbf{h}(\mathbf{x}_r)$ is smooth and $\mu_g(t)$ is C^1 continuous on $t \in [0, \infty)$, $\mathbf{h}_g(\mathbf{x}_r, t)$ is continuously differentiable for all $t \geq 0$. Now, the kinematic equation (10) is rewritten as

$$\dot{\mathbf{x}}_r = -\mu_g(t) [\mathbf{x}_r]_\times \mathbf{h}(\mathbf{x}_r). \quad (19)$$

Theorem 2: Consider the boresight kinematics described by (10). The extended guidance law $\boldsymbol{\Omega}_r = \mathbf{h}_g(\mathbf{x}_r, t)$, as defined in (18), ensures that the boresight vector \mathbf{x}_r converges to a small neighborhood around either the goal point \mathbf{x}^* or an undesired critical point \mathbf{c}_i within the prescribed time T_g^* .

Proof. The proof is relegated to Appendix C. ■

B. Prescribed-Time Boresight Tracking Control

By leveraging barrier and PPTA functions, we here propose a PTDO-based reduced-attitude tracking controller to achieve reference trajectory tracking within a prescribed time $T_c^* \leq T_g^*$, while ensuring that the boresight vector \mathbf{x} remains within a fixed-size ‘‘safe tube’’ around the reference trajectory \mathbf{x}_r . To facilitate the subsequent analysis, the reference trajectory $\mathbf{x}_r \in \mathbb{S}^2$, governed by (11) with $\boldsymbol{\Omega}_r$ defined in (18), is expressed in the body frame as

$$\boldsymbol{\sigma} := \mathbf{R}^\top \mathbf{x}_r \in \mathbb{S}^2$$

which is the *reduced attitude*.

The objective of boresight tracking is to align the boresight vector \mathbf{x} with the reference trajectory \mathbf{x}_r in the inertial frame. This is equivalent to stabilizing $\boldsymbol{\sigma}$ to the body-fixed boresight vector \mathbf{b} in the body frame. In the following, we formulate a tracking problem for reduced attitude and define the reduced-attitude tracking error in the body frame as

$$\begin{aligned} \sigma_e &= 1 - (\mathbf{x}_r^\top \mathbf{R})(\mathbf{R}^\top \mathbf{x}) \\ &= 1 - \boldsymbol{\sigma}^\top \mathbf{b}. \end{aligned} \quad (20)$$

Given the kinematics of (8) and (11), we apply the properties of cross product operator to the time derivative of σ_e , yielding the reduced-attitude tracking error kinematics

$$\begin{aligned} \dot{\sigma}_e &= -\mathbf{b}^\top (\dot{\mathbf{R}}^\top \mathbf{x}_r + \mathbf{R}^\top \dot{\mathbf{x}}_r) \\ &= -\mathbf{b}^\top ((\mathbf{R}[\boldsymbol{\omega}]_\times)^\top \mathbf{x}_r + \mathbf{R}^\top [\mathbf{h}_p]_\times \mathbf{R} \mathbf{R}^\top \mathbf{x}_r) \\ &= -\mathbf{b}^\top [\boldsymbol{\sigma}]_\times \boldsymbol{\omega}_e \end{aligned} \quad (21)$$

where $\boldsymbol{\omega}_e \in \mathbb{R}^3$ denotes the angular velocity error expressed in the body frame, defined as

$$\boldsymbol{\omega}_e := \boldsymbol{\omega} - \mathbf{R}^\top \mathbf{h}_p. \quad (22)$$

Then, applying (22) gets the error dynamics

$$\mathbf{J} \dot{\boldsymbol{\omega}}_e = \underbrace{-\mathbf{C} \boldsymbol{\omega}_e - \mathbf{G}}_H + \mathbf{u} + \mathbf{d} \quad (23)$$

with

$$\begin{aligned} \mathbf{C} &:= -[\mathbf{J}(\boldsymbol{\omega}_e + \mathbf{R}^\top \mathbf{h}_p)]_\times + ([\mathbf{R}^\top \mathbf{h}_p]_\times \mathbf{J} + \mathbf{J}[\mathbf{R}^\top \mathbf{h}_p]_\times) \\ \mathbf{G} &:= [\mathbf{R}^\top \mathbf{h}_p]_\times \mathbf{J} \mathbf{R}^\top \mathbf{h}_p + \mathbf{J} \mathbf{R}^\top \dot{\mathbf{h}}_p. \end{aligned}$$

Here, the augments of \mathbf{C} and \mathbf{G} are omitted for brevity.

A PTDO is designed to reconstruct the disturbance \mathbf{d} :

$$\begin{aligned} \dot{\mathbf{p}} = & -c_1\mu_c(t)\mathbf{p} - c_1\mu_c(t)(c_1\mu_c(t)\mathbf{J}\boldsymbol{\omega}_e + \mathbf{H} + \mathbf{u}) \\ & - c_1\dot{\mu}_c(t)\mathbf{J}\boldsymbol{\omega}_e \end{aligned} \quad (24)$$

$$\dot{\hat{\mathbf{d}}} = \mathbf{p} + c_1\mu_c(t)\mathbf{J}\boldsymbol{\omega}_e \quad (25)$$

where $c_1 > 0$ is a constant; $\mu_c(t)$ is a PPTA function defined in (4) with design parameters T_c and T_c^* ($T_c^* \leq T_g^*$); $\mathbf{p} \in \mathbb{R}^3$ is the internal state of the observer, and $\hat{\mathbf{d}} \in \mathbb{R}^3$ is the estimated disturbance. Define the estimation error as $\tilde{\mathbf{d}} := \mathbf{d} - \hat{\mathbf{d}}$. Using (24) and (25), the observation error dynamics is given by

$$\begin{aligned} \dot{\tilde{\mathbf{d}}} &= \dot{\mathbf{d}} - (\dot{\mathbf{p}} + c_1\mu_c(t)\mathbf{J}\dot{\boldsymbol{\omega}}_e + c_1\dot{\mu}_c(t)\mathbf{J}\boldsymbol{\omega}_e) \\ &= \dot{\mathbf{d}} - c_1\mu_c(t)\tilde{\mathbf{d}}. \end{aligned} \quad (26)$$

Theorem 3: Consider the reduced-attitude error dynamics described in (23). The PTDO given by (24) and (25) is PPTS in the sense that the estimation error $\tilde{\mathbf{d}}$ remains within the set $\|\tilde{\mathbf{d}}\| \leq \tilde{d}_m := \max\{d_m/c_1, \|\tilde{\mathbf{d}}(0)\|\}$ and converges to a small neighborhood of zero within the prescribed time T_c^* .

Proof. Consider the Lyapunov function candidate

$$V_d = \frac{1}{2}\tilde{\mathbf{d}}^\top \tilde{\mathbf{d}} \quad (27)$$

In view of (26), the time derivative of V_d is

$$\dot{V}_d = -c_1\mu_c(t)\tilde{\mathbf{d}}^\top \tilde{\mathbf{d}} + \tilde{\mathbf{d}}^\top \dot{\tilde{\mathbf{d}}}. \quad (28)$$

Using Young's inequality and Assumption 1, we have

$$\tilde{\mathbf{d}}^\top \dot{\tilde{\mathbf{d}}} \leq \frac{c_1\mu_c(t)}{2}\|\tilde{\mathbf{d}}\|^2 + \frac{1}{2c_1}d_m^2 \quad (29)$$

wherein we have used the fact that $\mu_c(t) \geq \mu_c(0) = 1$. Then, inserting (29) into (28) yields

$$\dot{V}_d \leq -c_1V_d + \frac{1}{2c_1}d_m^2 \quad (30)$$

from which it is clear that $\dot{V}_d \leq 0$ if $\|\tilde{\mathbf{d}}\| \geq d_m/c_1$, indicating that the set $\|\tilde{\mathbf{d}}\| \leq d_m/c_1$ is attractive and forward invariant. Therefore, $\tilde{\mathbf{d}}(t)$ remains within the set $\|\tilde{\mathbf{d}}\| \leq \tilde{d}_m$ for all $t \geq 0$. As per Lemma 1, it further follows from the first inequality of (30) that the PTDO is PPTS, in the sense that $\tilde{\mathbf{d}}$ converges to a small residual set within the prescribed time T_{ce} . ■

In the following, the PTDO is used to design the reduced-attitude tracking controller. Since a safety margin of size ε is incorporated into the design of boresight guidance law, if the condition $d_{S^2}(\boldsymbol{\sigma}(t), \mathbf{b}) < \varepsilon$ (equivalent to $d_{S^2}(\mathbf{x}(t), \mathbf{x}_r(t)) < \varepsilon$) holds for all $t \geq 0$, then the inertial-frame boresight vector $\mathbf{x}(t)$ remains outside all forbidden pointing zones. To ensure that $d_{S^2}(\boldsymbol{\sigma}(t), \mathbf{b}) < \varepsilon$ for all $t \geq 0$, the following constraint is imposed on σ_e :

$$\sigma_e(t) < \rho := 1 - \cos \varepsilon, \quad \forall t \geq 0. \quad (31)$$

This implies that, at each moment, the boresight vector $\mathbf{x}(t)$ is allowed to stay within a conical zone centered around the axis $\mathbf{x}_r(t)$, with a half-angle of ε . Unifying all such conical zones along t forms a fixed-size ‘‘safe tube’’ around $\mathbf{x}_r(t)$. To deal with this constraint, we define a transformed error

$$\xi(t) := \frac{\sigma_e(t)}{\rho} \quad (32)$$

whose governing equation is derived from (21) as

$$\dot{\xi}(t) = -\frac{1}{\rho}\mathbf{b}^\top[\boldsymbol{\sigma}]_\times\boldsymbol{\omega}_e. \quad (33)$$

It is evident from (32) that $0 \leq \xi(t) < 1$ is equivalent to (31), and $\xi(t) = 0$ only when $\sigma_e(t) = 0$. Therefore, the boresight tracking problem boils down to achieving practical prescribed-time convergence of $\xi(t)$, while ensuring $0 \leq \xi(t) < 1$ holds for all $t \geq 0$.

Let us define $\mathbf{z} := \boldsymbol{\omega}_e - \boldsymbol{\omega}_c$, where $\boldsymbol{\omega}_c \in \mathbb{R}^3$ is a virtual control law to be designed. Consider a barrier function $V_\xi = \ln \frac{1}{1-\xi}$. Taking its time derivative along (33) gets

$$\dot{V}_\xi = -\frac{1}{\rho(1-\xi)}\mathbf{b}^\top[\boldsymbol{\sigma}]_\times(\mathbf{z} + \boldsymbol{\omega}_c). \quad (34)$$

Design the virtual control law as

$$\boldsymbol{\omega}_c = -c_2\mu_c(t)[\boldsymbol{\sigma}]_\times\mathbf{b} \quad (35)$$

where $c_2 > 0$ is a constant. It is noted that $\mu_c(t)$ and $\boldsymbol{\sigma}$ are continuously differentiable, so does $\boldsymbol{\omega}_c$. Then, substituting (35) into (34), whilst recalling (20), we get

$$\begin{aligned} \dot{V}_\xi &= -\frac{c_2\mu_c(t)}{\rho(1-\xi)}(1 - (\mathbf{b}^\top\boldsymbol{\sigma})^2) - \frac{\mathbf{b}^\top[\boldsymbol{\sigma}]_\times\mathbf{z}}{\rho(1-\xi)} \\ &\leq -c_2(2 + \rho)\mu_c(t)V_\xi - \frac{\mathbf{b}^\top[\boldsymbol{\sigma}]_\times\mathbf{z}}{\rho(1-\xi)} \end{aligned} \quad (36)$$

where the fact that $1 + \mathbf{b}^\top\boldsymbol{\sigma} \geq 2 + \rho$ in the set $0 \leq \xi(t) < 1$ has been used.

In view of (9), the time derivative of \mathbf{z} is derived as

$$\mathbf{J}\dot{\mathbf{z}} = -\mathbf{J}\dot{\boldsymbol{\omega}}_c + \mathbf{H} + \mathbf{u} + \mathbf{d}. \quad (37)$$

Now design the reduced-attitude control law as

$$\mathbf{u} = -c_3\mu_c(t)\mathbf{z} + \mathbf{J}\dot{\boldsymbol{\omega}}_c - \mathbf{H} - \hat{\mathbf{d}} - \frac{[\boldsymbol{\sigma}]_\times\mathbf{b}}{\rho(1-\xi)} \quad (38)$$

where $c_3 > 0$ is a constant. Substituting (38) into (37) gets

$$\mathbf{J}\dot{\mathbf{z}} = -c_3\mu_c(t)\mathbf{z} + \tilde{\mathbf{d}} - \frac{[\boldsymbol{\sigma}]_\times\mathbf{b}}{\rho(1-\xi)}. \quad (39)$$

To facilitate the subsequent analysis, we define the closed-loop error as $\mathbf{Z} := [\xi, \mathbf{z}^\top, \tilde{\mathbf{d}}^\top]^\top \in \mathbb{R}^7$.

Theorem 4: Consider the reduced-attitude dynamics given by (9) and (10) under Assumption 1. The tracking controller (38), along with the PTDO defined by (24) and (25), ensures the following:

- 1) All closed-loop signals are bounded.
- 2) The reduced-attitude tracking error σ_e complies with the constraint defined by (31) at all times.
- 3) The closed-loop system is PPTS, in the sense that the error vector \mathbf{Z} converges to a small residual set within the prescribed time T_c^* .

Proof. Consider the Lyapunov function candidate

$$V = V_d + V_\xi + \frac{1}{2}\mathbf{z}^\top\mathbf{J}\mathbf{z} \quad (40)$$

Taking the time derivative of V along (30), (36), and (39) gets

$$\begin{aligned} \dot{V} &\leq -c_1\mu_c(t)V_d - c_2(2+\rho)\mu_c(t)V_\xi - \frac{c_3\mu_c(t)}{2}\|\mathbf{z}\|^2 \\ &\quad + \frac{1}{2c_3}\sup_{t\geq 0}\|\tilde{\mathbf{d}}(t)\|^2 + \frac{1}{2c_1}d_m^2 \\ &\leq -\alpha\mu_c(t)V + \beta \end{aligned} \quad (41)$$

where $\alpha := \min\{c_1, c_2(2+\rho), \frac{c_3}{\lambda_M(\mathbf{J})}\} > 0$ with $\lambda_M(\mathbf{J})$ being the maximum eigenvalue of \mathbf{J} , and $\beta := \frac{1}{2c_1}d_m^2 + \frac{1}{2c_3}\tilde{d}_m^2 > 0$. From (41), it follows that V is bounded according to Lemma 1. Then, one can conclude that V_ξ and all closed-loop signals are bounded. The boundedness of V_ξ implies that $0 \leq \xi(t) < 1$ for all $t \geq 0$, and consequently, the tracking error σ_e respects the constraint (31). According to Lemma 1, we conclude from (41) that the error vector \mathbf{Z} converges to a residual set within the prescribed time T_c^* . In particular, the set size can be made arbitrarily small by increasing T_c^* closer to T_c . ■

Remark 2: Under the proposed IBGC framework, if the tube radius ρ is less than the safety margin ϵ and the controller settling time T_c^* does not exceed the guidance time T_g^* , then the boresight vector \mathbf{x} will converge to a small neighborhood of the desired orientation \mathbf{x}^* within T_g^* , while avoiding all forbidden zones \mathcal{P}_i , $i \in \mathbb{I}$. Therefore, the proposed IBGC scheme achieves pointing-constrained boresight reorientation within a preassigned time tailored to specific task demands, in the presence of external disturbances.

IV. ILLUSTRATIVE EXAMPLE

In this section, a numerical example is provided to show the efficacy of the proposed IBGC scheme. The spacecraft inertia vector is $\mathbf{J} = [20, 1.2, 0.9; 1.2, 17, 1.4; 0.9, 1.4, 15]\text{kg}\cdot\text{m}^2$. The spacecraft is required to reorient the boresight vector \mathbf{x} (its expression in the body-fixed frame is $\mathbf{b} = [0, 0, 1]^\top$) of the onboard light-sensitive telescope from an initial pointing to the desired orientation $\mathbf{x}^* = [-0.939, -0.305, 0.1589]^\top$. The disturbance \mathbf{d} is modeled as

$$\mathbf{d} = 10^{-3} \times \begin{bmatrix} 3 \cos(0.2t) + 4 \sin(0.06t) - 1 \\ -1.5 \sin(0.04t) + 3 \cos(0.1t) + 1.5 \\ 3 \sin(0.2t) - 8 \sin(0.08t) + 1.5 \end{bmatrix} \text{Nm.}$$

During this maneuver, the boresight vector \mathbf{x} needs to avoid certain forbidden zones, with parameters listed in Table I. The task completion time is 150 s.

We begin by verifying the effectiveness of the prescribed-time guidance law $\boldsymbol{\Omega}_r = \mathbf{h}_g(\mathbf{x}_r, t)$ in (18), referred to as ‘PPT-BG’. For comparison, the baseline guidance law $\boldsymbol{\Omega}_r = \mathbf{h}(\mathbf{x}_r)$ in (15), denoted as ‘APF-BG’, is also simulated. The design parameters are tabulated in Table II. The guidance trajectories starting from a set of initial orientations in the inertial frame are depicted in Fig. 4. As observed, the PPT-BG successfully guides the boresight vector \mathbf{x}_r from various initial orientations to the goal, while avoiding all forbidden zones. Note that the APF-BG follows the same path as the PPT-BG, and thus its trajectory is not shown here. To quantify the alignment, let us define the boresight error as $x_s := 1 - \mathbf{x}_r^\top \mathbf{x}^*$. The comparison results of x_s and $\|\boldsymbol{\Omega}_r\|$ are depicted in Fig. 5, from which it is evident that the APF-BG only achieves asymptotic error

TABLE I
GEOMETRICAL DETAILS OF FORBIDDEN ZONES.

Forbidden zone	Central axis	Angle
\mathcal{P}_0	$\mathbf{f}_0 = -\mathbf{x}^*$	$\theta_0 = 2^\circ$
\mathcal{P}_1	$\mathbf{f}_1 = [0, -0.453, -0.8915]^\top$	$\theta_1 = 25^\circ$
\mathcal{P}_2	$\mathbf{f}_2 = [0, -0.951, 0.3092]^\top$	$\theta_2 = 25^\circ$
\mathcal{P}_3	$\mathbf{f}_3 = [0.275, 0.847, -0.4549]^\top$	$\theta_3 = 20^\circ$
\mathcal{P}_4	$\mathbf{f}_4 = [-0.769, 0.599, 0.2232]^\top$	$\theta_3 = 25^\circ$
\mathcal{P}_5	$\mathbf{f}_5 = [0.345, 0.475, 0.8095]^\top$	$\theta_3 = 20^\circ$

TABLE II
GUIDANCE AND CONTROL PARAMETERS.

Method	Parameter
PPTA function $\mu_g(t)$	$T_g = 150, T_g^* = 149$
PPTA function $\mu_c(t)$	$T_c = 15, T_c^* = 14$
PPT-BG in (18)	$\epsilon = \frac{\pi}{30}, \epsilon^* = \frac{\pi}{12}, k_a = 0.01, k_r = 0.1$
PPT-TC in (38)	$c_1 = c_2 = c_3 = 0.2, \rho = \epsilon, \mathbf{p}(0) = \mathbf{0}_3$
APF in [16]	$k_p = 5, k_d = 2$
PD in [7]	$k_p = 0.05, k_d = 2$

convergence, while the PPT-BG reaches a small neighborhood of the origin within the prescribed time $T_g^* = 149$ s, regardless of initial orientations. This result highlights the crucial role of the PPTA function $\mu_g(t)$ in enabling practical prescribed-time convergence of x_s . It is noted that a faster convergence rate is accompanied by a larger velocity norm, as evident in the left subfigures of Fig. 5.

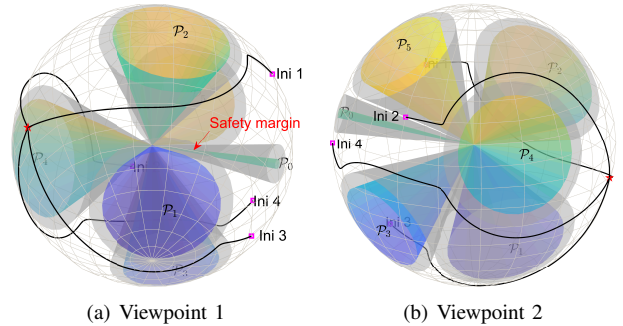


Fig. 4. Boresight trajectories on \mathbb{S}^2 in the inertial frame, where the purple squares denote different initial orientations and the red star is the desired orientation \mathbf{x}^* .

We next verify the proposed reduced-attitude tracking controller (38), referred to as ‘PPT-TC’. The controller parameters are detailed in Table II. As a case study, the guided trajectory starting from the 4th initial orientation is selected as the reference trajectory. The closed-loop responses are shown in Fig. 6. As can be seen, the proposed PPT-TC ensures that the output-tracking errors σ_e and ω_e , as well as the disturbance estimation error $\tilde{\mathbf{d}}$, converge to small residual sets within the prescribed time $T_c^* = 14$ s; moreover, it maintains σ_e within the preset ‘tube’ with a radius of $\rho = \epsilon$. Consequently, the boresight vector \mathbf{x} reaches a small neighborhood around the desired orientation \mathbf{x}^* within the prescribed time $T_g^* = 149$ s, while avoiding all forbidden zones, as shown in Fig. 7. This ensures successful completion of the boresight reorientation task within a required time of 150 s.

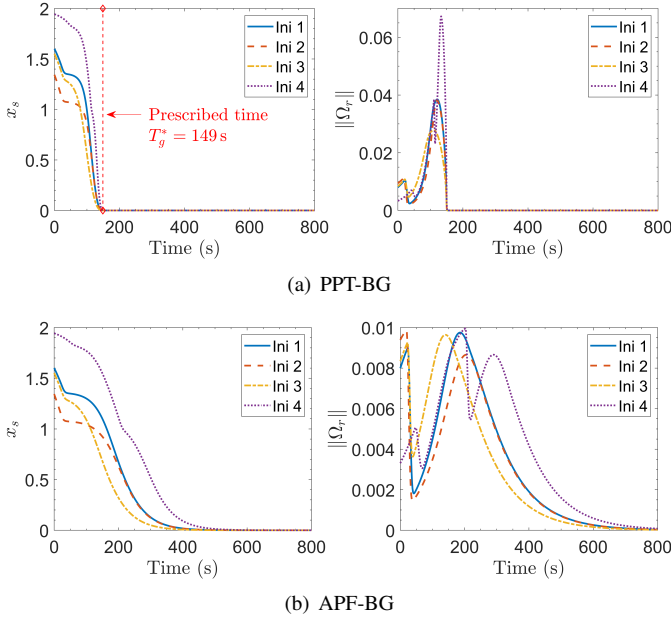


Fig. 5. Comparison of the responses of PPT-BG and APF-BG under four distinct initial orientations labeled as ‘Ini 1’ to ‘Ini 4’.

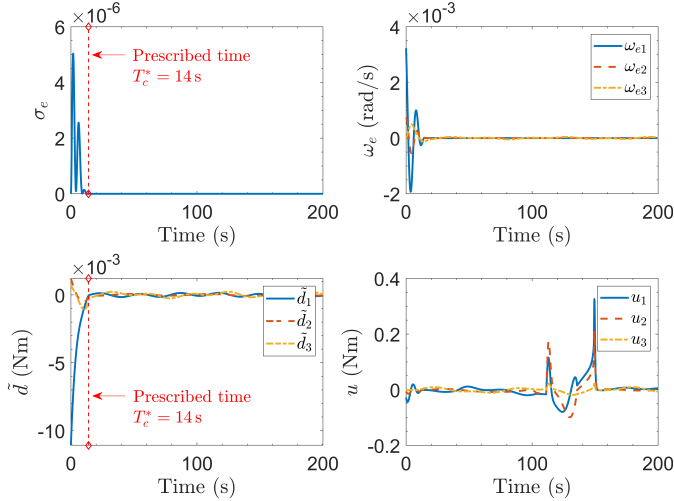


Fig. 6. Control responses of the proposed PPT-TC.

V. EXPERIMENTAL RESULTS

In this section, the hardware-in-the-loop (HIL) experiments are performed to demonstrate the practical effectiveness of the proposed IBGC scheme. The experimental setup is provided in Fig. 8. The testbed consists of the following main modules: 1) a high-performance simulation computer (HPRTSC), which runs the attitude dynamics on the VxWorks system; 2) a three-axis turntable for simulating the spacecraft attitude motion from the dynamics in HPRTSC; 3) a set of sensors including three grating encoders and four fiber-optic gyroscopes, which are mounted on the turntable and utilized for measuring Euler angles and angular velocities; 4) an actuator system consisting of three reaction wheels (RWs) and a control module that receives the torque signals from the controller in the HPRTSC and allocates corresponding torque commands to RWs. Each RW provides a maximum torque of 0.1 Nm and a maximum

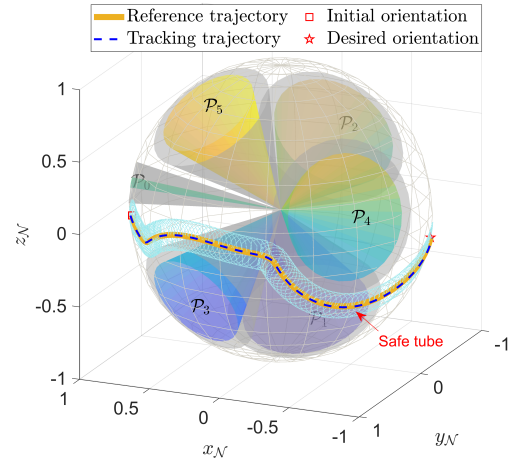


Fig. 7. Boresight tracking trajectory on S^2 .

speed of 5000 rpm.

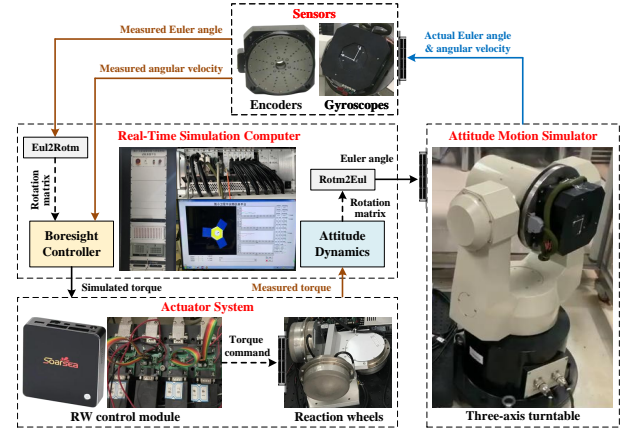


Fig. 8. Schematic of the HIL testbed.

To avoid the singularity that occurs when the pitch angle equals 90° , the initial value of the boresight vector is selected as $\mathbf{x}(0) = [0.809, 0.587, 0.0308]^\top$ (i.e., Ini 2 in Fig. 4). In addition, the nominal inertia matrix and the disturbance \mathbf{d} are given in Sec. IV. The inertia uncertainties caused by phenomena, such as payload motion and appendage deployment, are given by $\Delta \mathbf{J} = \text{diag}[0.2te^{-0.2\sqrt{t}}, 2e^{-0.1t}, 3e^{-0.1t+1}] \text{ kg} \cdot \text{m}^2$. Two classical reduced-attitude control methods are compared with the proposed IBGC method. The first is the APF-based controller introduced in [16] (referred to as ‘APF’), which is defined as $\mathbf{u} = -k_p \mathbf{R}^\top [\mathbf{x}]_\times \nabla U(\mathbf{x}) - k_d \boldsymbol{\omega}$. The second is the PD control introduced in [7] (referred to as ‘PD’), expressed as $\mathbf{u} = k_p \mathbf{R}^\top [\mathbf{x}]_\times \mathbf{x}_d - k_d \boldsymbol{\omega}$, where $k_p, k_d > 0$ are constant gains with values given in Table II.

The experimental results of the proposed IBGC scheme are shown in Fig. 9. It is evident that the boresight error, defined as $x_e := 1 - \mathbf{x}^\top \mathbf{x}^*$, converges to zero within the prescribed time $T_g^* = 149 \text{ s}$. This implies that the boresight vector \mathbf{x} achieves the desired orientation within the required time frame of 150 s. Furthermore, the torque outputs of the RWs remain within the magnitude limits. The comparison results are plotted in Fig. 10. As can be seen, both the APF and PD methods fail

to achieve boresight reorientation within the required 150 s. While it is possible to improve the convergence time of these two methods by increasing the control gains, this parameter selection process is often time-consuming. The 3D boresight trajectories for these three methods are presented in Fig. 11, from which it is clear that both IBGC and APF successfully avoid the forbidden pointing zones, whereas the PD controller fails. In summary, the experimental results demonstrate the practical effectiveness of the proposed IBGC scheme in terms of prescribed time and pointing avoidance.

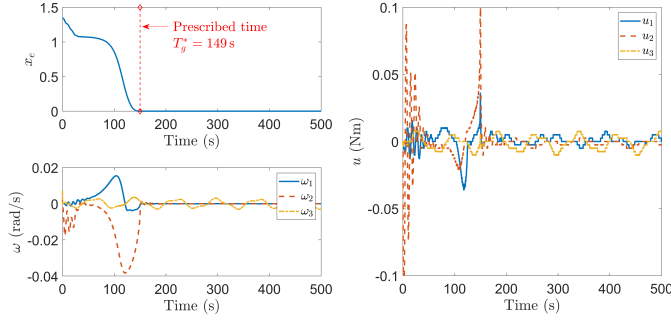


Fig. 9. Experimental responses of the proposed IBGC scheme.

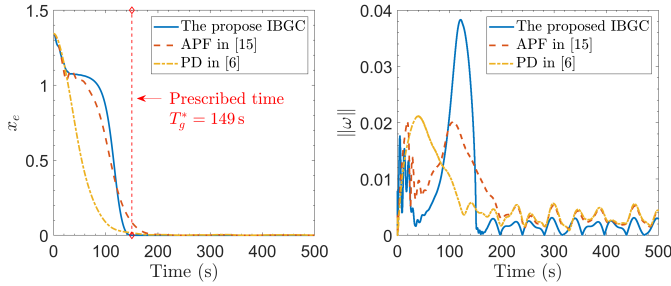


Fig. 10. Comparison of experimental results.

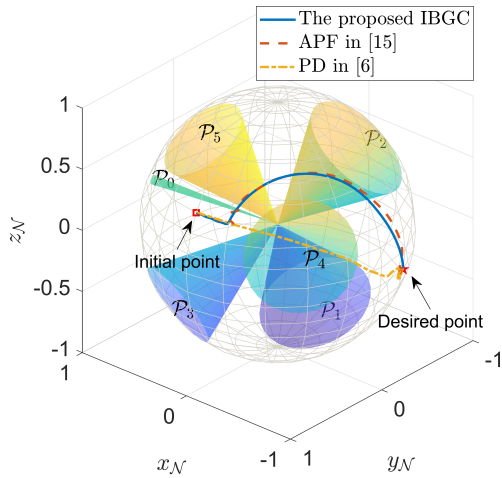


Fig. 11. Comparison of 3D boresight trajectories.

VI. CONCLUSIONS AND FUTURE WORKS

This article develops a PPTA function and integrates it into the IBGC scheme, providing a systematic and flexible control

framework to address the boresight orientation problem on \mathbb{S}^2 under temporal and pointing constraints. The salient features of the proposed method, as demonstrated through simulation and experimental results, are two-fold: 1) it achieves boresight reorientation within a finite time that can be arbitrarily preassigned according to the required task completion time, while ensuring that the boresight vector avoids all forbidden pointing zones; 2) it enables precise reconstruction of unknown disturbances within a prescribed time. For future work, we envisage extending our method to multi-spacecraft attitude coordination with explicit consideration of tempo-spatial constraints.

APPENDIX A

The proof is analyzed over two time intervals: $[0, T^*)$ and $[T^*, \infty)$. Consider the first time interval, in which $\mu(t) = \mu_p(t)$. Multiplying both sides of (5) by the integrating factor $(T-t)^{-\alpha T}$ yields

$$(T-t)^{-\alpha T} \frac{dV}{dt} + \alpha(T-t)^{-\alpha T} \mu(t)V \leq \beta(T-t)^{-\alpha T},$$

whose left-hand side can be expressed as

$$\frac{d}{dt} [(T-t)^{-\alpha T} V] \leq \beta(T-t)^{-\alpha T}. \quad (42)$$

Integrating both sides of (42) from 0 to T_e yields

$$(T-T^*)^{-\alpha T} V(\mathbf{y}(T^*)) \leq T^{-\alpha T} V_0 + \frac{\beta}{\alpha T - 1} [(T-T^*)^{1-\alpha T} - T^{1-\alpha T}]. \quad (43)$$

Therefore, the solution of the system (1) converges to the set $V(\mathbf{y}) \leq v_1$ at the prescribed time $t = T^*$.

We next consider the time interval $[T^*, \infty)$, where $\mu(t) \geq \mu(T^*) > 0$. From (5), it follows that

$$\dot{V} \leq -\alpha_s V + \beta \quad (44)$$

with $\alpha_s := \alpha \mu(T^*)$. Then, one can easily deduce that

$$V(\mathbf{y}(t)) \leq \left(V(\mathbf{y}(T^*)) - \frac{\beta}{\alpha_s} \right) e^{-\alpha_s(t-T^*)} + \frac{\beta}{\alpha_s}. \quad (45)$$

To proceed, two cases are discussed.

Case 1: $V(\mathbf{y}(T^*)) > v_2$. It follows from (45) that $V(\mathbf{y}(t))$ decreases exponentially to the set $V(\mathbf{y}) \leq v_2$. This, together with the fact that $V(\mathbf{y}(T^*)) \leq v_1$, ensures that $\mathbf{y}(t)$ remains within the set $V(\mathbf{y}) \leq v_1$ for all $t \geq T^*$.

Case 2: $V(\mathbf{y}(T^*)) \leq v_2$. Inspecting (44) finds that $\dot{V}(\mathbf{y}) = 0$ on the level set $V(\mathbf{y}) = v_2$. This implies that the set $V(\mathbf{y}) \leq v_2$ is forward invariant. Thus, from the fact that $V(\mathbf{y}(T^*)) \leq v_2$, it follows that $V(\mathbf{y}(t)) \leq v_2$ for all $t \geq T^*$.

With the above two cases in mind, one can easily conclude that $\mathbf{y}(t)$ remains within the set Ω given by (6) for all $t \geq T^*$. Furthermore, given that $T - T^* \ll \alpha T - 1$, it is evident from (7) that the size of the set Ω can be artificially reduced by increasing T^* closer to T . This completes the proof. ■

APPENDIX B

Taking the time derivative of $U(\mathbf{x}_r)$ along (16) yields

$$\begin{aligned}\dot{U}(\mathbf{x}_r) &= -\nabla U(\mathbf{x}_r)^\top [\mathbf{x}_r]_\times [\mathbf{x}_r]_\times^\top \nabla U(\mathbf{x}_r) \\ &= -\|[\mathbf{x}_r]_\times^\top \nabla U(\mathbf{x}_r)\|^2 \leq 0\end{aligned}$$

which implies that $U(\mathbf{x}_r)$ is bounded. Thus, we have $\mathbf{x}_r(t) \in \mathcal{F}_\epsilon$ for all $t \geq 0$ and $\mathbf{x}_r(0) \in \mathcal{F}_\epsilon$, that is, the practical free space \mathcal{F}_ϵ is forward invariant. Applying LaSalle's invariance principle, we further conclude that the solution of (16) asymptotically converges to the set of critical points, given by

$$\text{Crit } U := \{\mathbf{x}_r \in \mathbb{S}^2 \mid [\mathbf{x}_r]_\times^\top \nabla U(\mathbf{x}_r) = \mathbf{0}\}.$$

It is easy to verify that $[\mathbf{x}_r]_\times^\top \nabla U(\mathbf{x}_r) = \mathbf{0}$ holds if and only if \mathbf{x}_r and $\nabla U(\mathbf{x}_r)$ are collinear, or $\nabla U(\mathbf{x}_r) = \mathbf{0}$. Given that $\mathbf{x}^* \in \mathbb{S}^2 \setminus \bigcup_{i=0}^m \mathcal{I}_i$ and $\nabla \phi_i(\mathbf{x}_r^\top \mathbf{f}_i) \geq 0$, it follows from (14) that $\nabla U(\mathbf{x}_r) \neq \mathbf{0}$, thus precluding the latter condition. Next, we consider two cases to analyze the former one.

Case 1: $\mathbf{x}_r \in \mathbb{S}^2 \setminus \bigcup_{i=0}^m \mathcal{I}_i$, indicating that \mathbf{x}_r remains outside the influence regions of all forbidden pointing constraints. In this case, we have $\nabla \phi_i(\mathbf{x}_r^\top \mathbf{f}_i) = 0$ for all $i \in \mathbb{I}$. Then, the gradient $\nabla U(\mathbf{x}_r)$ given by (14) reduces to $\nabla U(\mathbf{x}_r) = -k_a \mathbf{x}^*$. Solving $[\mathbf{x}_r]_\times^\top \nabla U(\mathbf{x}_r) = k_a [\mathbf{x}_r]_\times \mathbf{x}^* = \mathbf{0}$ yields $\mathbf{x}_r = \pm \mathbf{x}^*$. However, since $-\mathbf{x}^* \in \mathcal{P}_0$ by construction, the only feasible solution is the desired equilibrium $\mathbf{x}_r = \mathbf{x}^*$.

Case 2: $\mathbf{x}_r \in \mathcal{I}_i$, $i \in \mathbb{I}$. As the influence regions of pointing constraints are pairwise disjoint, it is sufficient to examine the critical points for each pointing constraint \mathcal{P}_i separately. Then, $[\mathbf{x}_r]_\times^\top \nabla U(\mathbf{x}_r) = \mathbf{0}$ is equivalent to (17). As $\mathbf{x}^* \in \mathbb{S}^2 \setminus \bigcup_{i=0}^m \mathcal{I}_i$ and $-\mathbf{x}^* \in \mathcal{P}_0$, it is evident that $[\mathbf{x}_r]_\times \mathbf{x}^* \neq \mathbf{0}$ for $\mathbf{x}_r \in \mathcal{I}_i$, $i \in \mathbb{I}$. According to the property of $\nabla \phi_i(\cdot)$, we have that $\nabla \phi_i(\mathbf{x}_r^\top \mathbf{f}_i) \geq 0$, with equality holding only when $\mathbf{x}_r^\top \mathbf{f}_i = \varepsilon_i^*$. Given this, (17) requires that $\mathbf{x}_r^\top \mathbf{f}_i < \varepsilon_i^*$, and that the vectors $[\mathbf{x}_r]_\times \mathbf{x}^*$ and $[\mathbf{x}_r]_\times \mathbf{f}_i$ have the same direction. As shown in Fig. 12(a), $[\mathbf{x}_r]_\times \mathbf{x}^*$ points in the opposite direction to the vector $[\mathbf{x}_r]_\times \mathbf{f}_0$ for all $\mathbf{x}_r \in \text{int}(\mathcal{I}_0)$, indicating that no critical points exist in the set $\mathbf{x}_r \in \mathcal{I}_0$. We next consider the case $\mathbf{x}_r \in \mathcal{I}_i$, $i \in \mathbb{I} \setminus \{0\}$, where the critical points (if they exist) lie on the plane spanned by \mathbf{x}^* and \mathbf{f}_i , specifically on the side of \mathbf{f}_i opposite to \mathbf{x}^* , as shown in Fig. 12(b). This condition ensures that $[\mathbf{x}_r]_\times \mathbf{x}^*$ and $[\mathbf{x}_r]_\times \mathbf{f}_i$ point in the same direction. We thus only need to determine whether the magnitude of both sides of (17) are equal. Since $d_{\mathbb{S}^2}(\mathbf{x}_r, \mathbf{x}^*) < \pi$ and $d_{\mathbb{S}^2}(\mathbf{x}_r, \mathbf{f}_i) < \pi$, (17) implies that

$$k_a \frac{\sin(d_{\mathbb{S}^2}(\mathbf{x}_r, \mathbf{x}^*))}{\sin(d_{\mathbb{S}^2}(\mathbf{x}_r, \mathbf{f}_i))} = k_r \nabla \phi_i(\mathbf{x}_r^\top \mathbf{f}_i). \quad (46)$$

We note that the left-hand side of (46) varies within a bounded interval $(0, d_i]$ with some $d_i > 0$, whereas the right-hand side monotonically increases from 0 to ∞ , as $\mathbf{x}_r^\top \mathbf{f}_i$ increases from ε_i^* to ε_i . This implies that, for each forbidden zone \mathcal{P}_i , $i \in \mathbb{I} \setminus \{0\}$, there certainly exists a single critical point $\mathbf{x}_r = \mathbf{c}_i$ that satisfies (46) (equivalent to (17)). ■

APPENDIX C

The proof is analyzed over two time intervals $[0, T_g^*)$ and $[T_g^*, \infty)$, separately.

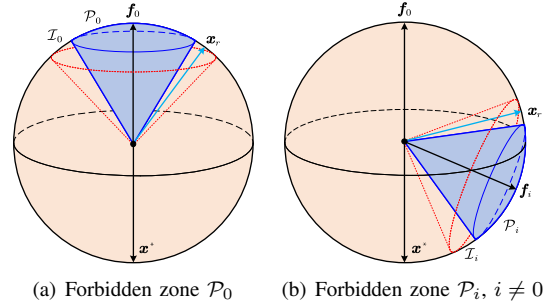


Fig. 12. Illustration of potential critical points for i -th forbidden zone.

1) Consider the interval $t \in [0, T_g^*)$. Let us define $t := \eta(s)$ (a TST function in Definition 2), $\bar{\mathbf{x}}_r(s) := \mathbf{x}_r(t) = \mathbf{x}_r(\eta(s))$. Then, the kinematics (19) can be rewritten in a stretched time interval $s \in [0, s_g)$ as

$$\bar{\mathbf{x}}_r'(s) := \frac{d\bar{\mathbf{x}}_r(s)}{ds} = \frac{d\mathbf{x}_r(\eta(s))}{d\eta(s)} \cdot \frac{d\eta(s)}{ds} \quad (47)$$

where $s_g := \eta^{-1}(T_g^*) = -T_g \ln(1 - T_g^*/T_g)$ is a constant. It is evident that $s_g \rightarrow +\infty$ as $T_g^* \rightarrow T_g$. With (3) and (19) in mind, (47) reduces to

$$\begin{aligned}\bar{\mathbf{x}}_r'(s) &= -\mu_g(\eta(s)) [\mathbf{x}_r(\eta(s))]_\times \mathbf{h}(\mathbf{x}_r(\eta(s))) \eta'(s) \\ &= -[\bar{\mathbf{x}}_r(s)]_\times \mathbf{h}(\bar{\mathbf{x}}_r(s))\end{aligned} \quad (48)$$

where the facts that $\mu_g(t) = \mu_p(t)$ for all $t \in [0, T_g^*)$ and that $\mu_p(\eta(s))\eta'(s) = 1$ have been used. As per Definition 2, we have $\eta(0) = 0$ and $\mu_p(0) = 1$, from which it follows that $\bar{\mathbf{x}}_r(0) = \mathbf{x}_r(0)$ and $\bar{\mathbf{x}}_r'(0) = \dot{\mathbf{x}}_r(0)$. Therefore, the solution of (48) is equivalent to that of the kinematics (16). In Theorem 1, we have demonstrated that the solution of (16) asymptotically converges to the set $\{\mathbf{x}^*\} \cup \bigcup_{i=1}^m \{\mathbf{c}_i\}$, indicating that $\bar{\mathbf{x}}_r(s)$ will converge to a neighborhood of either the desired equilibrium \mathbf{x}^* or an undesired critical point \mathbf{c}_i ($i \in \mathbb{I} \setminus \{0\}$) within the stretched time interval $s \in [0, s_g)$. Moreover, as s_g increases (by setting T_g^* closer to T_g), the neighborhood size decreases. Note that $\mathbf{x}_r(t) = \bar{\mathbf{x}}_r(s)$ and $t \rightarrow T_g^*$ as $s \rightarrow s_g$. Then, it can be claimed that $\mathbf{x}_r(t)$ converges to a neighborhood of either \mathbf{x}^* or \mathbf{c}_i within the prescribed time T_g^* . Furthermore, inspecting Theorem 1 reveals that $\bar{\mathbf{x}}_r(s) \in \mathcal{F}_\epsilon$ for all $s \in [0, s_g)$, allowing us to conclude that $\mathbf{x}_r(t)$ remains within the practical free space \mathcal{F}_ϵ for all $t \in [0, T_g^*)$. Actually, the solution of (19) on the interval $t \in [0, T_g^*)$ follows the same path as that obtained by the baseline guidance law on $s \in [0, s_g)$.

2) Next, consider the interval $t \in [T_g^*, \infty)$. Since $\mu_g(t) \geq \mu_p(T_g^*) > 1$, $\forall t \geq T_g^*$ holds due to Property 1, the trajectory $\mathbf{x}_r(t)$, governed by (19), will continuously and asymptotically converge to either the desired equilibrium \mathbf{x}^* or the undesired critical point \mathbf{c}_i , while avoiding all forbidden pointing zones. This is evident from the proof of Theorem 1.

Synthesizing the above analyses allow us to conclude Theorem 2. This completes the proof. ■

REFERENCES

- [1] S. Gao, X. Liu, Y. Jing, and G. M. Dimirovski, "Finite-time prescribed performance control for spacecraft attitude tracking," *IEEE/ASME Transactions On Mechatronics*, vol. 27, no. 5, pp. 3087–3098, 2022.

- [2] H. Yang, Q. Hu, H. Dong, X. Zhao, and D. Li, "Optimized data-driven prescribed performance attitude control for actuator saturated spacecraft," *IEEE/ASME Transactions on Mechatronics*, vol. 28, no. 3, pp. 1616–1626, 2023.
- [3] X. Shao, Q. Hu, Y. Shi, and Y. Zhang, "Fault-tolerant control for full-state error constrained attitude tracking of uncertain spacecraft," *Automatica*, vol. 151, p. 110907, 2023.
- [4] Q. Meng, H. Yang, and B. Jiang, "Second-order sliding-mode on SO(3) and fault-tolerant spacecraft attitude control," *Automatica*, vol. 149, p. 110814, 2023.
- [5] X. Shao, Q. Hu, D. Li, Y. Shi, and B. Yi, "Composite adaptive control for anti-unwinding attitude maneuvers: An exponential stability result without persistent excitation," *IEEE Transactions on Aerospace and Electronic Systems*, vol. 59, no. 2, pp. 1051–1066, 2022.
- [6] F. Bullo, R. M. Murray, and A. Sarti, "Control on the sphere and reduced attitude stabilization," *IFAC Proceedings Volumes*, vol. 28, no. 14, pp. 495–501, 1995.
- [7] N. A. Chaturvedi, A. K. Sanyal, and N. H. McClamroch, "Rigid-body attitude control," *IEEE Control Systems Magazine*, vol. 31, no. 3, pp. 30–51, 2011.
- [8] C. M. Pong and D. W. Miller, "Reduced-attitude boresight guidance and control on spacecraft for pointing, tracking, and searching," *Journal of Guidance, Control, and Dynamics*, vol. 38, no. 6, pp. 1027–1035, 2015.
- [9] K. Spindler, "Attitude maneuvers which avoid a forbidden direction," *Journal of Dynamical and Control Systems*, vol. 8, no. 1, pp. 1–22, 2002.
- [10] Q. Shen, C. Yue, C. H. Goh, B. Wu, and D. Wang, "Rigid-body attitude stabilization with attitude and angular rate constraints," *Automatica*, vol. 90, pp. 157–163, 2018.
- [11] J. Yang, Y. Duan, M. K. Ben-Larbi, and E. Stoll, "Potential field-based sliding surface design and its application in spacecraft constrained reorientation," *Journal of Guidance, Control, and Dynamics*, vol. 44, no. 2, pp. 399–409, 2021.
- [12] Z. Kang, Q. Shen, S. Wu, and C. J. Damaren, "Saturated attitude control of multispacecraft systems on so (3) subject to mixed attitude constraints with arbitrary initial attitude," *IEEE Transactions on Aerospace and Electronic Systems*, vol. 59, no. 5, pp. 5158–5173, 2023.
- [13] X. Tan, S. Berkane, and D. V. Dimarogonas, "Constrained attitude maneuvers on SO(3): Rotation space sampling, planning and low-level control," *Automatica*, vol. 112, p. 108659, 2020.
- [14] F. Celani and D. Lucarelli, "Spacecraft attitude motion planning using gradient-based optimization," *Journal of Guidance, Control, and Dynamics*, vol. 43, no. 1, pp. 140–145, 2020.
- [15] R. Calaon and H. Schaub, "Constrained attitude maneuvering via modified-rodriques-parameter-based motion planning algorithms," *Journal of Spacecraft and Rockets*, vol. 59, no. 4, pp. 1342–1356, 2022.
- [16] Q. Hu, B. Chi, and M. R. Akella, "Reduced attitude control for boresight alignment with dynamic pointing constraints," *IEEE/ASME Transactions on Mechatronics*, vol. 24, no. 6, pp. 2942–2952, 2019.
- [17] X. Shao, Q. Hu, Z. H. Zhu, and Y. Zhang, "Fault-tolerant reduced-attitude control for spacecraft constrained boresight reorientation," *Journal of Guidance, Control, and Dynamics*, vol. 45, no. 8, pp. 1481–1495, 2022.
- [18] Y. Liu, Q. Hu, and G. Feng, "Adaptive reduced attitude control for rigid spacecraft with elliptical pointing constraints," *IEEE Transactions on Aerospace and Electronic Systems*, vol. 59, no. 4, pp. 3835–3847, 2023.
- [19] Y. Liu, H. Li, R. Lu, Z. Zuo, and X. Li, "An overview of finite/fixed-time control and its application in engineering systems," *IEEE/CAA Journal of Automatica Sinica*, vol. 9, no. 12, pp. 2106–2120, 2022.
- [20] X. Zhang, Q. Zong, L. Dou, R. Zhang, B. Tian, and W. Liu, "Finite-time distributed attitude synchronization for multiple spacecraft with angular velocity and input constraints," *IEEE Transactions on Control Systems Technology*, vol. 30, no. 4, pp. 1612–1624, 2022.
- [21] B. Jiang, Q. Hu, and M. I. Friswell, "Fixed-time attitude control for rigid spacecraft with actuator saturation and faults," *IEEE Transactions on Control Systems Technology*, vol. 24, no. 5, pp. 1892–1898, 2016.
- [22] B. Li, T. Guan, X. Guan, K. Zhang, and K.-F. C. Yiu, "Optimal fixed-time sliding mode control for spacecraft constrained reorientation," *IEEE Transactions on Automatic Control*, 2023.
- [23] A. J. Munoz-Vazquez, J. D. Sánchez-Torres, E. Jimenez-Rodriguez, and A. G. Loukianov, "Predefined-time robust stabilization of robotic manipulators," *IEEE/ASME Transactions on Mechatronics*, vol. 24, no. 3, pp. 1033–1040, 2019.
- [24] T. Yucelen, Z. Kan, and E. Pasiliao, "Finite-time cooperative engagement," *IEEE Transactions on Automatic Control*, vol. 64, no. 8, pp. 3521–3526, 2018.
- [25] C. Hua, P. Ning, and K. Li, "Adaptive prescribed-time control for a class of uncertain nonlinear systems," *IEEE Transactions on Automatic Control*, vol. 67, no. 11, pp. 6159–6166, 2021.
- [26] X. Chen, Y. Wang, Y. Wang, and Y. Song, "Time axis shifting finite-gain-based prescribed-time tracking control under nonvanishing disturbances," *IEEE Transactions on Industrial Electronics*, vol. 71, no. 12, pp. 16 368–16 376, 2024.
- [27] W. Cheng, K. Zhang, and B. Jiang, "Fixed-time and prescribed-time fault-tolerant optimal tracking control for heterogeneous multiagent systems," *IEEE Transactions on Automation Science and Engineering*, vol. 21, no. 4, pp. 7275–7286, 2024.
- [28] P. Ning, S. N. Dashkovskiy, C. Hua, and K. Li, "Dual-gain function based prescribed-time output feedback control nonlinear time-delay systems," *SIAM Journal on Control and Optimization*, vol. 62, no. 4, pp. 2254–2272, 2024.
- [29] A.-M. Zou, Y. Liu, Z.-G. Hou, and Z. Hu, "Practical predefined-time output-feedback consensus tracking control for multiagent systems," *IEEE Transactions on Cybernetics*, vol. 53, no. 8, pp. 5311–5322, 2022.
- [30] D. Swaroop, J. K. Hedrick, P. P. Yip, and J. C. Gerdes, "Dynamic surface control for a class of nonlinear systems," *IEEE Transactions on Automatic Control*, vol. 45, no. 10, pp. 1893–1899, 2000.
- [31] A. Shakouri and N. Assadian, "Prescribed-time control for perturbed euler-lagrange systems with obstacle avoidance," *IEEE Transactions on Automatic Control*, vol. 67, no. 7, pp. 3754–3761, 2021.